

CoFe₂O₄ nanoparticles as efficient bifunctional catalysts applied in Zn–air battery

Jie Yin

State Key Laboratory of Applied Organic Chemistry, Key Laboratory of Nonferrous Metal Chemistry and Resources Utilization of Gansu Province, College of Chemistry and Chemical Engineering, Lanzhou University, Lanzhou 730000, People's Republic of China

Liang Shen

China National Nuclear Corporation Lanzhou Uranium Enrichment Co. Ltd., Manage and Plan Department, Lanzhou 730000, People's Republic of China

Yuxuan Li, Min Lu, Ke Sun, and Pinxian Xi^{a)}

State Key Laboratory of Applied Organic Chemistry, Key Laboratory of Nonferrous Metal Chemistry and Resources Utilization of Gansu Province, College of Chemistry and Chemical Engineering, Lanzhou University, Lanzhou 730000, People's Republic of China

(Received 2 August 2017; accepted 19 September 2017)

The transition metal compound catalysts have been taken a great part in renewable energy conversion and storage systems. Herein, we report the uniform CoFe₂O₄ nanoparticles with abundant oxygen vacancies and specific active surface exposed through the simple hydrothermal reaction for improving the electrocatalytic performance and stability. They show good electrocatalytic performance for hydrogen evolution reaction in 0.5 M H₂SO₄ with an onset potential of 20 mV, the overpotential of 45 mV (at $j = 10 \text{ mA/cm}^2$), and remarkable long-term stability more than 100 h at different current densities and better oxygen reduction reaction activity with lower overpotential in 0.1 M KOH. Moreover, the home-made primary Zn–air batteries, using CoFe₂O₄ nanoparticles as an air–cathode display the high open-circuit voltage of 1.47 V and the maximum power density of 142 mW/cm². The two-series-connected batteries fabricated by CoFe₂O₄ nanoparticles can support a light-emitting diode to work for more than 48 h.

I. INTRODUCTION

Hydrogen evolution reaction (HER) and oxygen reduction reaction (ORR) are of great interest due to their important roles in renewable energy conversion and storage systems.^{1–3} High-performance of HER and ORR is limited due to the activity of the catalysts.^{4–6} Traditionally, precious metals (e.g., platinum) are efficient for HER and ORR with both activity and stability.^{7–9} However, their high cost and scarcity have hindered their large-scale application.^{10–13} What is more, the design of an ideal electrocatalyst that can drive both HER and ORR with high current density at low overpotential and long-term stability is still a challenge.^{14–16} To address these challenging issues, many efforts have been focused on non-precious-metal-based materials such as perovskite, metallic oxide, and their derivatives as bifunctional electrocatalysts,^{15–20} as exploring strategies to develop more efficient and stable catalysts in a cost-effective manner is still a technological task in the development of energy conversion and storage systems.

The development of energy conversion and storage systems take an important part in daily life because of the energy crisis and ecological environment pollution. Metal–air batteries as potential alternative energy sources have been the subject of intense investigation in recent years.^{21–25} Theoretically, Zn–air batteries, as one of most widespread metal–air batteries, have high energy density (1086 W h/kg, including oxygen) and low cost and are environmentally friendly.^{25–30} However, the obtained electrochemical performances are still far from satisfying because the energy efficiency is still limited by the large overpotentials derived from the sluggish oxygen reduction and evolution reaction (ORR/OER) kinetics, the unstable electrode structure even further fueling it.^{31–33} Therefore, the development of excellent air electrode with high catalytic activity, good conductivity, and favorable mechanical properties is of great importance in enhancing the energy density, powder density, and rechargeable capacity for the Zn–air batteries.

Among various transition metal compound catalysts, the spinel AB₂O₄ (A, B = metal) possesses high electrochemical activity and superior adsorption and activation of electroactive species, which can be attributed to surface redox active metal centers by electron transition between different valence states of metals in O-sites.^{34–36}

Contributing Editor: Chuan Zhao

^{a)}Address all correspondence to this author.

e-mail: xipx@lzu.edu.cn

DOI: 10.1557/jmr.2017.404

As one of the most intriguing spinel composite oxides, CoFe₂O₄ is widely used because of many advantages, including low cost, high abundance, low toxicity, and rich redox chemistry.^{36–38} CoFe₂O₄ also displays a boosting electrocatalytic performance due to the abundant metal ions with different valence states (e.g., Fe²⁺, Fe³⁺, Co²⁺, Co³⁺). As we all know, various morphologies of CoFe₂O₄ have been researched in many fields.^{38–40} However, the performance of CoFe₂O₄ is still limited by morphology and active crystal face exposed. Recently, many researches have been devoted to fabricating the more active and uniform nanocrystals. Furthermore, many studies revealed that crystal face such as (100), (110), and (111) with low surface energy have been well documented in literature.

Herein, we report the uniform CoFe₂O₄ nanoparticles with abundant oxygen vacancies and the specific active surface exposed as active and stable bifunctional electrocatalysts for boosting HER and ORR through a simple hydrothermal method. The high electrocatalytic activities of the CoFe₂O₄ nanoparticles for HER and ORR are caused by their uniform nanoparticle morphology, the active crystal face (111) and (110) exposed, and abundant oxygen vacancies. As expected, they show excellent performance for both HER in both acidic and basic media and ORR in 0.1 M KOH. In detail, they show superior activity for HER in acid media with an onset potential of 20 mV, overpotential of 45 mV (at $j = 10 \text{ mA/cm}^2$), remarkable long-term stability more than 100 h with different current densities, and rapid kinetic reaction with the lower Tafel slope of 35 mV/dec. What is more, the CoFe₂O₄ nanoparticles also displayed a better performance for HER in basic media with an overpotential of 65 mV (at $j = 10 \text{ mA/cm}^2$). The bifunctional electrocatalytic capacity of CoFe₂O₄ nanoparticles was confirmed by good performance for ORR. Both the onset potential (0.84 V) and half-wave potential (0.67 V) of the CoFe₂O₄ nanoparticles for ORR are closer to that of Pt/C (20%), and more importantly, the ORR is catalyzed by the CoFe₂O₄ nanoparticles via four electrons processes. Based on the bifunctional electrocatalytic performance, the primary home-made Zn–air batteries were fabricated, using CoFe₂O₄ nanoparticles as the air–cathode. More interestingly, the two-series-connected batteries fabricated by CoFe₂O₄ nanoparticles can support a light-emitting diode (LED) to work for more than 48 h.

II. EXPERIMENTAL SECTION

A. Materials

Fe(NO₃)₃·9H₂O (98.0%), Co(NO₃)₂·6H₂O (99.0%), NaCH₃COO (99.0%), H₂SO₄ (99.0%), KOH (90.0%), and polyethylene glycol 200 (PEG-200) (90.0%) were purchased from Aladdin Nafion (5%; Los Angeles, California) and carbon black was purchased from

Sigma-Aldrich (St. Louis, Missouri) and Pt/C catalyst (20 wt% Pt on carbon black) from Premetek Co. (Wilmington, Delaware); all of these materials are of analytical grade and without further purification. The deionized (DI) water for solution preparation was obtained from a Millipore Autopure system (18.2 MΩ, Millipore Ltd., Billerica, Massachusetts). The 0.5 M H₂SO₄, and 0.1 and 1.0 M KOH were used as the electrolyte in the electrochemical experiment.

B. Fabrication of CoFe₂O₄ nanoparticles

The CoFe₂O₄ nanoparticles were prepared by a facile hydrothermal synthesis method. Generally speaking, Fe(NO₃)₃·9H₂O (10 mmol, 4.0401 g), Co(NO₃)₂·6H₂O (5 mmol, 1.4553 g), and NaCH₃COO (30 mmol 2.46 g) were dissolved in 40 mL of polyethylene glycol 200 (PEG-200). The clear solution of these materials was obtained after stirring for about 30 min. Then the solution was transferred into the Teflon-lined stainless steel (80 mL) in an autoclave. After autoclave treatment at 200 °C for 16 h, the autoclave was allowed to cool down to room temperature. The resulting precipitates were filtered and washed thoroughly with DI water and ethanol more than three times and then dried in air at 80 °C for 12 h. These precipitates were calcined in air at 400 °C for 2 h to obtain CoFe₂O₄ nanoparticles.

C. Structure characterization

X-ray diffraction (XRD) experiments were conducted by the X'Pert Pro X-ray diffractometer with Cu K_α radiation ($\lambda = 0.1542 \text{ nm}$) under a voltage of 40 kV from 20° to 90°. Transmission electron microscopy (TEM) and high-resolution TEM (HRTEM) specimens were prepared by depositing a drop of the CoFe₂O₄ nanoparticles dispersion in H₂O on copper grids coated with amorphous carbon. TEM and HRTEM observations were performed under an acceleration voltage of 200 kV with a JEOL JEM 2100 TEM (JEOL, Ltd., Tokyo, Japan). X-ray photoelectron spectroscopy (XPS) analyses were made with a VG ESCALAB 220I-XL device (VG Instruments, Middlewich, United Kingdom) and corrected with C 1s line at 284.6 eV.

D. The electrocatalytic performance test

All the electrochemical measurements were carried out in a typical three-electrode system consisting of a glass carbon working electrode, a Pt auxiliary electrode, and an Ag/AgCl reference electrode (3 M KCl) connected to a CHI 760 E electrochemical workstation (CHI Instruments, Shanghai Chenhua Instrument Corp., Shanghai, China) at a scan rate of 2 mV/s in the electrolyte solution. The potentials were referenced to the reversible hydrogen electrode (RHE) through RHE calibration [$E(\text{RHE}) = E(\text{Ag/AgCl}) + 0.0951 \text{ pH} + 0.197$]. Also, a resistance

test was made, and the iR compensation was applied using the CHI software. In this work, all electrochemical experiments were conducted at 20 ± 0.2 °C. The working electrodes were prepared in the same way for both HER and ORR. First, the catalysts (3 mg) were dispersed in a *N,N*-dimethylformamide (DMF) solution (1470 μ L) with 30 μ L of Nafion solution (Aldrich, 5 wt%) by sonication for at least 40 min to form a homogeneous ink. Then, 7 μ L of the dispersion was loaded onto a glassy carbon electrode with a diameter of 3 mm (loading 0.2 mg/cm²), and 12.6 μ L of the dispersion was loaded onto the rotating disk electrode (RDE) or rotating ring-disk electrode (RRDE) with a diameter of 4 mm (loading 0.2 mg/cm²). The electrochemical measurements for ORR were conducted on RRDE at 1600 rpm in oxygen-saturated 0.1 M KOH solution. The RDE was measured at rotating rates varying from 400 to 2400 rpm at the scan rate of 2 mV/s. The relationship between the measured currents (*j*) with various rotating speeds (ω) under fixed potentials can be expressed on the basis of the Koutechky–Levich (K–L) equation⁴¹:

$$1/j = 1/j_k + 1/(B\omega^{1/2}) \quad , \quad (1)$$

where j_k is the kinetic current and ω is the electrode rotating rate. *B* is determined from the slope of the K–L plots based on the Levich equation below:

$$B = 0.2nF(D_{O_2})^{2/3}v^{-1/6}C_{O_2} \quad , \quad (2)$$

where *n* represents the transferred electron number per oxygen molecules. D_{O_2} is the diffusion coefficient of O₂ in 0.1 M KOH ($D_{O_2} = 1.9 \times 10^{-5}$ cm²/s). *v* is the kinetic viscosity ($v = 0.01$ cm²/s). C_{O_2} is the bulk concentration of O₂ ($C_{O_2} = 1.2 \times 10^{-6}$ mol/cm³). The constant 0.2 is adopted when the rotation speed is expressed in rpm.

For the RRDE measurements, catalyst inks and electrodes were prepared by the same method as for RDE. The disk electrode was scanned at a rate of 5 mV/s, and the ring potential was constant at 1.3 V versus RHE. The % OH₂[−] and transfer number (*n*) were determined by the following equations⁴¹:

$$\% \text{OH}_2^- = 200(I_r/N)/(I_d + I_r/N) \quad , \quad (3)$$

$$n = 4I_d/(I_d + I_r/N) \quad , \quad (4)$$

where I_d is disk current, I_r is ring current, and *N* is current collection efficiency of the Pt ring. *N* was determined to be 0.40.

E. Battery test

The Zn–air battery was assembled by the zinc plate anode and air–cathode. The air–cathode was prepared by

dropping the CoFe₂O₄ nanoparticle homogeneous catalyst ink on the carbon fiber paper (CFP) and drying in air. First, the catalysts (9 mg) were dispersed in a DMF solution (4410 μ L) with 120 μ L of Nafion solution (Aldrich, 5 wt%) by sonication for at least 40 min to form a homogeneous ink. Then, 4 mL of the dispersion was loaded onto the CFP with 1×2 cm² (loading 2 mg/cm²). Last, the catalyst could be dried in air. The 6.0 M KOH was used as the electrolyte. All the Zn–air batteries were tested under ambient atmosphere. The polarization curve measurements were performed by linear scan voltammogram (LSV) (2 mV/s) at 25 °C with CHI 760 E electrochemical working station (CH Instrument).^{5,11}

III. RESULTS AND DISCUSSION

A. Synthesis and characterization of CoFe₂O₄ nanoparticles

A strategy was developed to synthesize CoFe₂O₄ nanoparticles by the hydrothermal method at 200 °C for 16 h (Experimental Section).⁴² Figure 1(a) shows the XRD pattern of the CoFe₂O₄ nanoparticles. The diffraction peaks of CoFe₂O₄ nanoparticles belong to the space groups of *F*43*m* (JCPDS Card No. 1-1121; $a = b = c = 8.39$ Å) with cubic structure. In detail, as shown in Fig. 1(a), the main crystal face of CoFe₂O₄ could be obviously seen, such as the (220) crystal face at the angle of 30.39°, the (311) crystal face at the angle of 35.78°, the (400) crystal face at the angle of 43.53°, the (511) crystal face at the angle of 57.18°, and the (440) crystal face at the angle of 62.74°, respectively. The morphology and structure of the CoFe₂O₄ nanoparticles were confirmed by TEM. As shown in Fig. 1(b), the TEM results reveal that the CoFe₂O₄ nanoparticles have uniform nanoparticles morphology with 5–10 nm. Furthermore, the HRTEM was used to study the exposed crystal face of the CoFe₂O₄ nanoparticles. As shown in Fig. 1(c), two clearly identified lattice fringe spaces of 2.97 and 4.86 Å correspond to the (220) plane and (111) plane exposed for the CoFe₂O₄ nanoparticles. Based on the above analysis, the CoFe₂O₄ nanoparticles with uniform small nanoparticles morphology and active crystal face exposed will have an excellent performance for electrocatalysis.

XPS measurements were also used to investigate the surface properties of the CoFe₂O₄ nanoparticles. In Fig. 1(d), the Co 2*p* spectrum of CoFe₂O₄ nanoparticles consists of two spin–orbit doublets characteristic of Co²⁺ and Co³⁺ and shakeup satellites (identified as “Sat.”), which can be observed at 795.48 eV for Co 2*p*_{1/2} peaks and 779.78 eV Co 2*p*_{3/2} with spin–orbit splitting of 15.7 eV. Additionally, there is a shake-up satellite peak at 786.55 eV.^{43,44} The energy gap of Co is about 8.93 eV which can be calculated by the difference value of binding energy between the Co 2*p* main peak and the satellite peak, meaning the Co cation holds a valence of Co³⁺.³³ Similarly, the Fe 2*p* spectrum

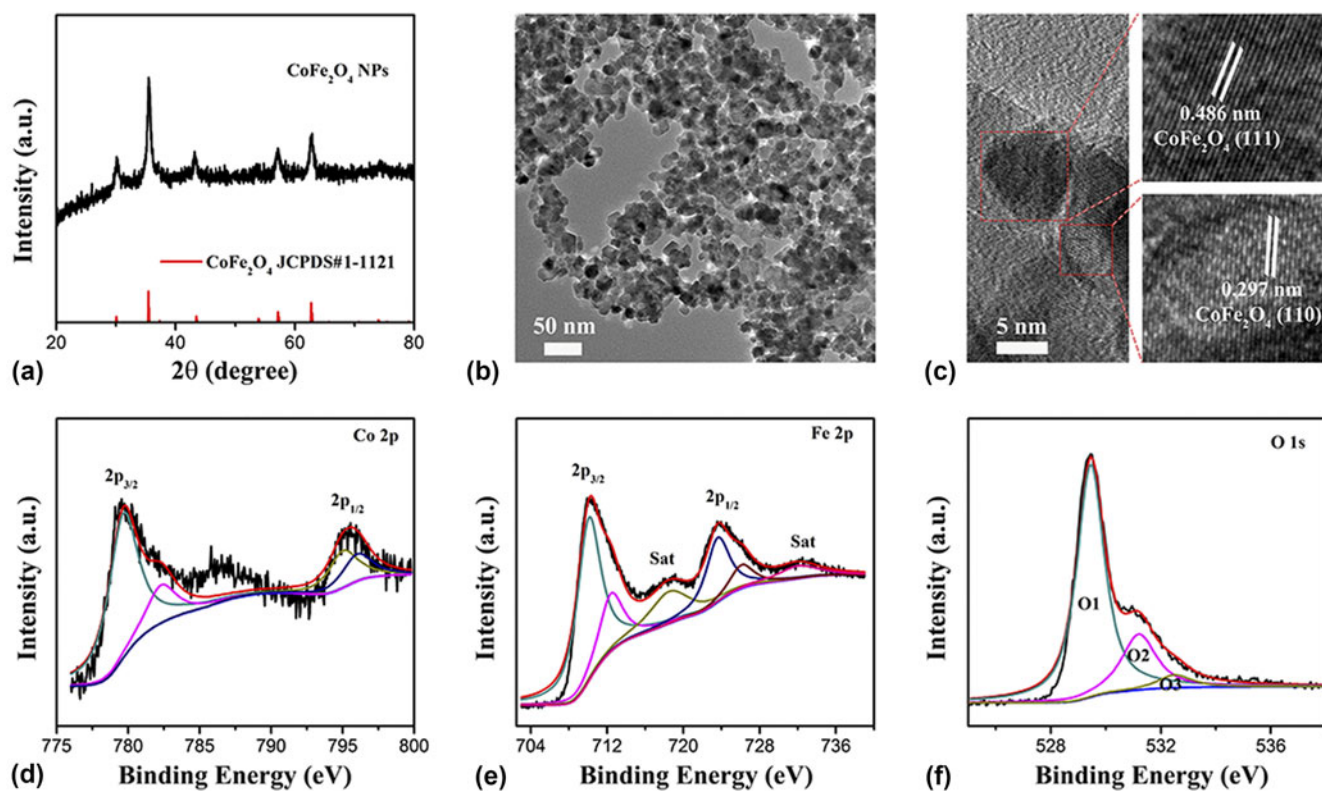


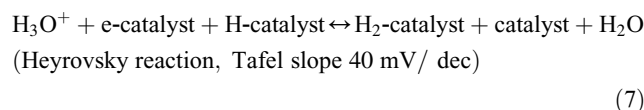
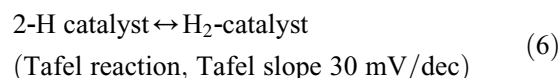
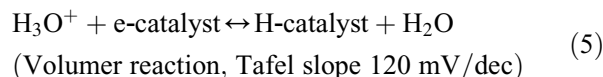
FIG. 1. (a) XRD patterns, (b) TEM, and (c) HRTEM images of CoFe₂O₄ nanoparticles. XPS spectra of (d) Co 2*p*, (e) Fe 2*p*, and (f) O 1*s* for the CoFe₂O₄ nanoparticles.

of CoFe₂O₄ nanoparticles [Fig. 1(e)] also consist of two spin–orbit peaks and corresponding Sat. of Fe²⁺ at high field and of Fe³⁺ at low field. Two main peaks located at 723.73 and 710.30 eV are Fe 2*p*_{1/2} and Fe 2*p*_{3/2} with the corresponding Sat. at 732.08 eV and 718.65 eV,^{45,46} respectively. Figure 1(f) shows the O1*s* spectrum of CoFe₂O₄ nanoparticles. In detail, it shows three oxygen contributions, denoted as O1 (529.46 eV) for oxygen atoms bound to metals (O-Fe/Co), O2 (531.22 eV) attributed to the oxygen vacancy (O_v), and O3 (532.52 eV) connected with surface-adsorbed water molecules (O–H₂O).⁴⁷ Extensive studies reveal that highly active nanostructures with abundant oxygen vacancies play an important role in enhancing the performance of the electrocatalytic reaction and renewable-energy devices due to their beneficial adsorption energy of the intermediate reaction, favorable desorption energy of the products, and efficient proton electron conduction. The CoFe₂O₄ nanoparticles with uniform small nanoparticles morphology, exposed active crystal face, and abundant oxygen vacancies will have an excellent performance for electrocatalysis and renewable-energy devices.

B. Hydrogen evolution reaction catalytic performance

The HER activity of the CoFe₂O₄ nanoparticles and commercial Pt/C (20 wt% Pt on carbon black from

Premetek. Co., mass loading of 0.2 mg/cm²) was confirmed by LSV both in acidic and basic media with the scan rate of 2 mV/s (Experimental Section).⁴⁸ Figure 2(a) shows that the CoFe₂O₄ nanoparticles exhibit the onset potential of 20 mV (versus RHE) slightly higher than that of commercial Pt/C (20%) (0 V versus RHE), and the overpotential of 45 mV (at *j* = 10 mA/cm²) a little more than that of commercial Pt/C (20%) (14 mV versus RHE), indicating that the catalytic behavior of the CoFe₂O₄ nanoparticles is similar to that of the commercial Pt/C catalyst.⁴⁹ Figure 2(b) displays the Tafel plots (log *j* ~ η) of HER. The mechanism typically involves three major reactions for hydrogen evolution in acid solutions on metal electrode surfaces.³⁵



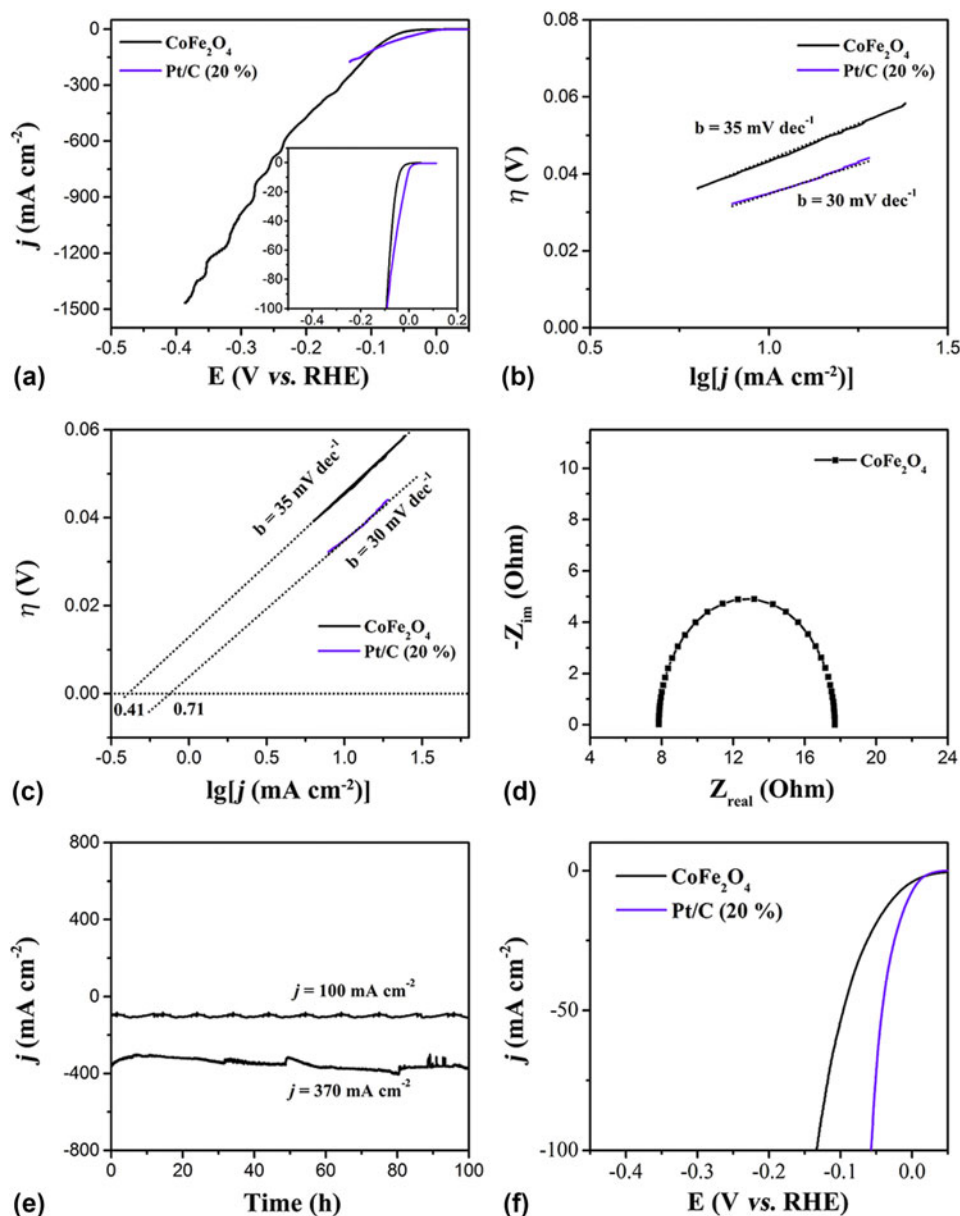


FIG. 2. (a) LSV curves of CoFe₂O₄ nanoparticles and Pt/C (20%) for hydrogen evolution in 0.5 M H₂SO₄, (b) the corresponding Tafel curves, and (c) the exchange current densities. (d) The Nyquist plot of the CoFe₂O₄ nanoparticles for HER. (e) HER stability tests of the CoFe₂O₄ nanoparticles at a different potential. (f) LSV curves of the samples for hydrogen evolution in 1 M KOH.

In these reaction processes, the metal-bound electrons are named e-catalyst, and a hydrogen atom or molecule adsorbed on to the surface of the metal atom catalysts is denoted as a H-catalyst or H₂-catalyst, respectively. These reactions are dependent on the inherent (electro)chemical and electronic properties of the catalyst surface. Generally, two main pathways are observed in HER, which are Volmer–Tafel reaction [Eqs. (5) and (6)] and Volmer–Heyrovsky reaction [Eqs. (5) and (7)]. In this work, the HER on the Pt/C (20%) with a Tafel slope of 30 mV/dec follows the known Tafel mechanism (H_{ads} + H_{ads} → H₂↑).⁵⁰ Similarly, the CoFe₂O₄ nanoparticles have a very

close Tafel slope of 35 mV/dec to that of Pt/C (20%), suggesting that the HER on this catalyst is dominated by the Heyrovsky mechanism (H₂O + MH_{ad} ⇌ M + H₂ + OH⁻) with electrochemical desorption step as the rate-determining step.⁵¹ Noticeably, the CoFe₂O₄ nanoparticles show an excellent performance for HER in acid media. In addition to the exchange current densities (*j*₀) of the CoFe₂O₄ nanoparticles and Pt/C (20%), the most inherent measure of HER activity was further calculated by extrapolating the Tafel plots to assess the quality of the electrocatalysts. As seen in Fig. 2(c), the *j*₀ value of 0.41 mA/cm² for the CoFe₂O₄ nanoparticles is slightly

less than the value of 0.71 mA/cm² for Pt/C (20%). Meanwhile, electrochemical impedance spectroscopy (EIS) was tested in 0.5 M H₂SO₄ solution to provide further insight into the electrode kinetics of the CoFe₂O₄ nanoparticles during the HER process. The Nyquist plot for the CoFe₂O₄ nanoparticles was measured in the 0.5 M H₂SO₄ solution from 0.01 to 100,000 Hz at 0.1 V. Circuit model fitting analysis of the EIS suggests that both electrodes can be modeled using a modified equivalent circuit consisting of a series resistance (R_s), a constant phase element, and a charge transfer resistance (R_{ct}). Figure 2(d) reveals that the R_{ct} of CoFe₂O₄ nanoparticles is only $\sim 10 \Omega$, which is a very small observed R_{ct} value, suggesting that the CoFe₂O₄ nanoparticles catalyst possesses a rapid electron transport during the HER process. The high j_0 value and the small R_{ct} signal suggest that the CoFe₂O₄ nanoparticles act as a promoter, facilitating the charge transfer on the surface to achieve efficient conversion of H⁺ into H₂ bubbles.

Stability as another important factor in all electrocatalytic reactions was also measured. As shown in Fig. 2(c), because of the uniform nanoparticles morphology, the exposed active crystal face of (111) and (220), and the abundant oxygen vacancies, the CoFe₂O₄ nanoparticles showed a superior stability for HER no less than 100 h at different current densities of 100 and 370 mA/cm. Many research have studied the HER performance of various catalysts in acid media, but the overall water splitting usually takes place in basic media. Therefore, the HER performance of the CoFe₂O₄ nanoparticles in basic media was also confirmed. As shown in Fig. 2(c), the CoFe₂O₄ nanoparticles show a remarkable activity for HER. Furthermore, the performance of CoFe₂O₄ nanoparticles for HER in basic media was also confirmed. The CoFe₂O₄ nanoparticles show better performance for HER in 1.0 M KOH solution with an overpotential of 65 mV at $j = 10$ mA/cm closer to that of Pt/C (20%). Based on the above analysis, the CoFe₂O₄ nanoparticles show an excellent performance for HER in both acidic and basic media.

The superior HER catalytic performance of the CoFe₂O₄ nanoparticle electrodes can be attributed to the uniform small nanoparticle structure, the exposed active crystal face of (111) and (220), and the abundant oxygen vacancies. First, the uniform small nanoparticle structure of materials is very important in electrocatalysis. Second, the exposed active crystal face of (111) and (220) for the CoFe₂O₄ nanoparticles endows low surface energy and better adsorption energy during the electrocatalytic reaction. Third, benefiting from the abundant oxygen vacancies, the reaction kinetics of HER can be significantly promoted. Also, these excellently provide a straightway path for electron transport and enhance structural stability. Therefore, the collaborative advantages enable CoFe₂O₄ nanoparticles to achieve excellent HER catalytic activity.

C. Oxygen reduction reaction catalytic performance

The electrocatalytic performance of the CoFe₂O₄ nanoparticles for the ORR was further measured to confirm the bifunctional electrocatalytic capacity and potential application in renewable energy technologies. The as-synthesized CoFe₂O₄ nanoparticles were coated on a RDE to investigate the ORR performance in an aqueous solution of 0.1 M KOH (Experimental Section). Meanwhile, the ORR electrocatalytic activity of commercial Pt/C (20%) was also tested as a contrast.⁵² Figure 3(a) shows the LSV curves measured at a rotating speed of 1600 rpm; these results indicate that the ORR catalytic activity of CoFe₂O₄ nanoparticles is comparable to the Pt/C catalyst with only slightly more negative onset potential [the CoFe₂O₄ nanoparticles: 0.84 V, Pt/C (20%): 0.95 V] and half-wave potential [the CoFe₂O₄ nanoparticles: 0.67 V, Pt/C (20%): 0.78 V]. The Tafel slopes of the CoFe₂O₄ nanoparticles and Pt/C (20%) were also tested to study the kinetics for the ORR. As shown in Fig. 3(b), the Tafel slopes of catalysts for ORR with the CoFe₂O₄ nanoparticles display the Tafel slope of 101 mV/dec higher than that of Pt/C (20%) (60 mV/dec), suggesting a lower reaction kinetics of the CoFe₂O₄ nanoparticles for ORR.

More importantly, the ORR performance of the CoFe₂O₄ nanoparticles was tested at different rotating speeds from 400 to 2400 rpm to study the relationship between the measured current densities (j) and various rotating speeds under fixed potentials. As shown in Fig. 3(c), the onset potential of the CoFe₂O₄ nanoparticles for ORR was the same as 0.84 V at different rotating speeds, but the half-wave potential has a slight difference at different rotating speeds such as 0.65 V at the rotating speeds of 400 rpm, 0.66 V at the rotating speeds of 800 rpm, 0.67 V at the rotating speeds of 1200 rpm, 0.68 V at the rotating speeds of 2000 rpm, and 0.69 V at the rotating speeds of 2400 rpm. However, the limited current densities have an obvious difference for every rotating speed, for example, 3.11 mA/cm² at rotating speeds of 400 rpm, 4.11 mA/cm² at rotating speeds of 800 rpm, 4.84 mA/cm² at rotating speeds of 1200 rpm, 5.34 mA/cm² at rotating speeds of 1600 rpm, 5.85 mA/cm² at rotating speeds of 2000 rpm, and 6.34 mA/cm² at rotating speeds of 2400 rpm, suggesting the better active performance at a higher rotating speed [Fig. 3(c)].

Based on the analysis about the relationship of current densities and various rotating speeds, the K–L plots of CoFe₂O₄ nanoparticles for ORR was calculated [Eqs. (1) and (2) in the Experimental Section].^{53–55} As shown in Fig. 3(d), the K–L equation at three different potentials was calculated. In detail, at 0.5 V, the calculated kinetic current densities were 0.429 mA/cm² at rotating speeds of 400 rpm, 0.348 mA/cm² at rotating speeds of 800 rpm, 0.308 mA/cm²

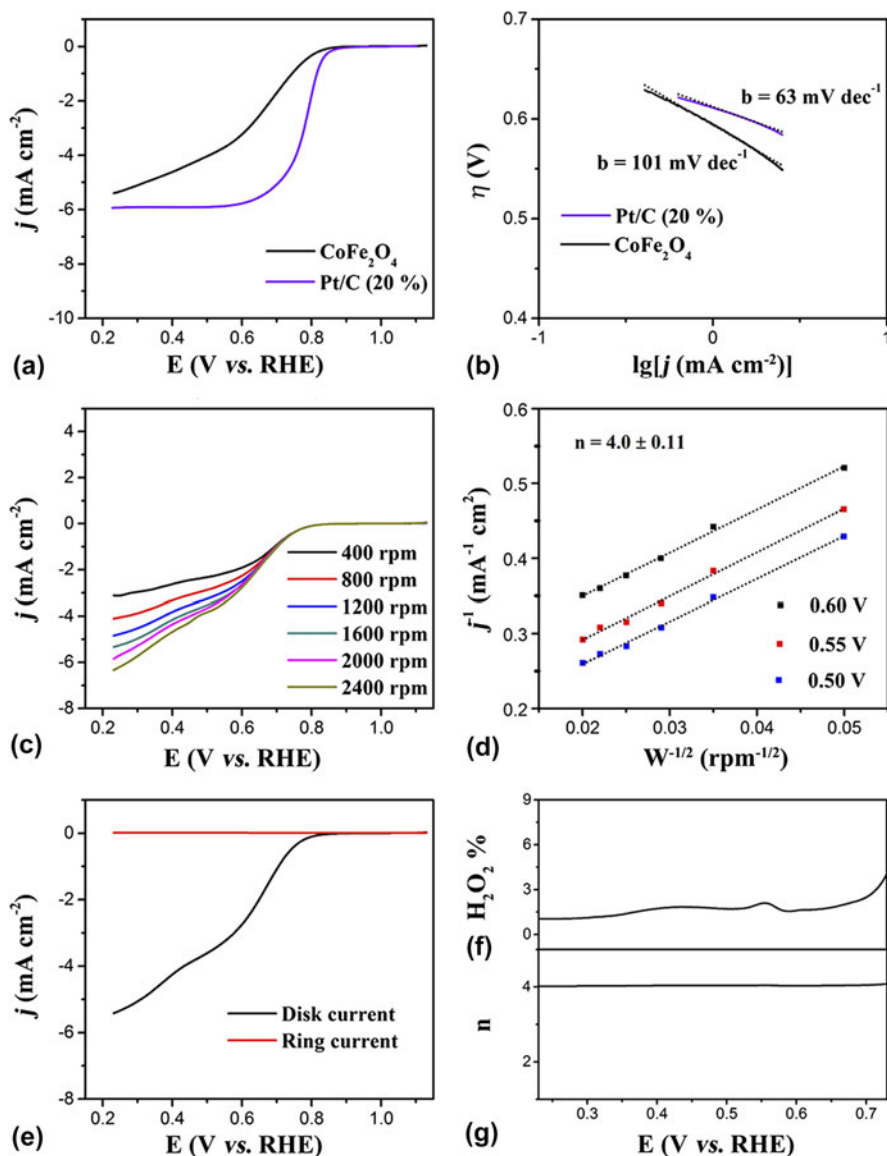


FIG. 3. (a) LSV curves of CoFe₂O₄ nanoparticles and Pt/C (20%) catalyst in O₂-saturated 0.1 M KOH solution and (b) corresponding Tafel curves. (c) LSV curves of the CoFe₂O₄ nanoparticles in O₂-saturated 0.1 M KOH with different rotating speeds. (d) The K–L plots for CoFe₂O₄ nanoparticles at a different potential. (e) RRDE measurements for the CoFe₂O₄ nanoparticles electrode in O₂-saturated 0.1 M KOH. (f) Percentage of peroxide and (g) the number of electron transfer in the total oxygen reduction progress.

at rotating speeds of 1200 rpm, 0.283 mA/cm² at rotating speeds of 1600 rpm, 0.273 mA/cm² at rotating speeds of 2000 rpm, and 0.261 mA/cm² at rotating speeds of 2400 rpm. When the potential was set at 0.55 V, the calculated kinetic current densities were slightly enhanced, such as 0.465 mA/cm² at rotating speeds of 400 rpm, 0.383 mA/cm² at rotating speeds of 800 rpm, 0.340 mA/cm² at rotating speeds of 1200 rpm, 0.315 mA/cm² at rotating speeds of 1600 rpm, 0.308 mA/cm² at rotating speeds of 2000 rpm, and 0.292 mA/cm² at rotating speeds of 2400 rpm. Furthermore, the larger kinetic current densities can be obtained at 0.6 V, such as 0.521 mA/cm² at rotating speeds of 400 rpm, 0.442 mA/cm² at rotating

speeds of 800 rpm, 0.400 mA/cm² at rotating speeds of 1200 rpm, 0.377 mA/cm² at rotating speeds of 1600 rpm, 0.360 mA/cm² at rotating speeds of 2000 rpm, and 0.351 mA/cm² at rotating speeds of 2400 rpm, respectively. More importantly, according to the K–L equation yield the electron transferred number (*n*) of the CoFe₂O₄ nanoparticles for ORR was calculated to approximately 4 at different potential. Based on the above analysis, the CoFe₂O₄ nanoparticles showed an outstanding performance for ORR.

Furthermore, the RRDE measurements were also used to study the ORR performance for CoFe₂O₄ nanoparticles electrode. First, just the same with RDE measurement,

the same uniform mass of CoFe₂O₄ nanoparticle catalyst ink was coated on the RRDE. Then, ORR took place on disk electrode and peroxide generation created on the Pt ring electrode which is set at a constant potential of 1.3 V versus RHE (Experimental Section). Fortunately, under the accurate measurement experiment, the CoFe₂O₄ nanoparticles exhibit good performance for ORR with a large disk current density and negligible current information of peroxide generation [Fig. 3(e)]. In addition, the percentage of peroxide generation during ORR progress was calculated from the RRDE data [Eq. (3) in the Experimental Section] and is lower than 10% from the potential from 0.23 to 0.73 V, indicating that during the ORR progress, the peroxide generation could be negligible [Fig. 3(f)]. Similarly, as shown in Fig. 3(g), the electron transferred number during the ORR progress is approximately 4, according to the RRDE data calculated results [Eq. (4) in the Experimental Section]. Thus, both the RDE and RRDE measurements suggest an efficient oxygen reduction directly into water via a four-electron pathway. As is well known, excellent catalytic properties are determined by a highly active structure. The excellent ORR catalytic performance of the CoFe₂O₄ nanoparticle electrodes can be attributed to the uniform small nanoparticle structure, the exposed active crystal face of

(111) and (220), and the abundant oxygen vacancies. Except for the uniform small nanoparticle structure, the abundant oxygen vacancies have an important role during the ORR progression for the CoFe₂O₄ nanoparticles. First, the oxygen vacancy is conducive to the adsorption of hydroxyl radicals in the basic media and reducing the adsorption energy at the same time, suggesting the active and fast electrocatalytic performance for ORR. Additionally, the exposed active crystal face of (111) and (220) for the CoFe₂O₄ nanoparticles also have a nonnegligible effect for ORR. Therefore, these collaborative advantages enable the CoFe₂O₄ nanoparticles to achieve excellent HER and ORR catalytic activity and stability. Based on the above experiment and analysis, the uniform CoFe₂O₄ nanoparticles with abundant oxygen vacancies and exposed active crystal face of (111) and (220) show excellent electrocatalytic performance for both HER and ORR and would have a better performance in renewable energy conversion and storage systems.

D. Battery performance

Considering the excellent bifunctional catalytic activity of the CoFe₂O₄ nanoparticles for both HER and ORR,

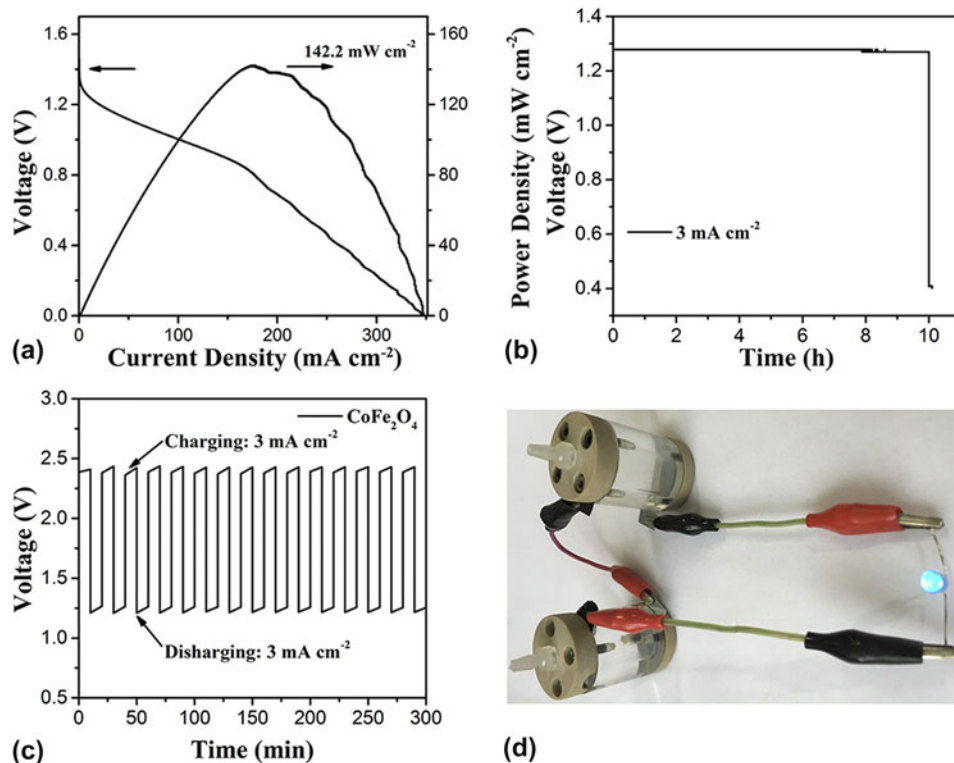


FIG. 4. (a) Discharge voltage curve and the corresponding power density plot of CoFe₂O₄ nanoparticles tested in the Zn–air battery. (b) Battery cycling test at charging and discharging current density of 3 mA/cm² in a short interval (10 min per cycle) for CoFe₂O₄ nanoparticles. (c) Discharge curves of the primary Zn–air battery with CoFe₂O₄ nanoparticles as the air cathode at 3 mA/cm². (d) Photograph of a blue LED (~3.0 V) powered by two-series-connected liquid Zn–air batteries.

a home-made primary Zn–air battery was assembled to further identify its performance under practical battery operation conditions. In detail, the battery uses the zinc plate as the anode, the CoFe₂O₄ nanoparticles coated on the CFP as the air–cathode, and 6.0 M KOH as the electrolyte (Experimental Section).^{54–56} Figure 4(a) shows the voltages and powder densities with current densities. When the current density is zero, the Zn–air battery using CoFe₂O₄ nanoparticles as air–cathode shows the open-circuit voltage (OCV) of 1.47 V. The CoFe₂O₄ nanoparticles-based Zn–air battery displayed good discharge capacity with 1 mA/cm² at 1.33 V, 3 mA/cm² at 1.30 V, and 5 mA/cm² at 1.28 V, respectively. The CoFe₂O₄ nanoparticles-based Zn–air battery can work stably and shows better power densities at different current densities, such as 12.45 mW/cm² at 10 mA/cm² and 55.91 mW/cm² at 50 mA/cm², and the maximum power densities is 142 mW/cm² at 175 mA/cm² [Fig. 4(a)]. Furthermore, the CoFe₂O₄ nanoparticles-based Zn–air battery was made as a commercial product. First, a transparent two opening can was made with an inner diameter of 1 cm and height of 3 cm. Secondly, two matched covers were built for the can, and one of the covers had a spiracle which served as the air collector. Then, the zinc plate and CoFe₂O₄ nanoparticles-based air–cathode should be fixed. Galvanostatic discharge measurements were conducted at different current densities to study the rechargeable capacity and stability [Fig. 4(b)]. Those Zn-air batteries show a voltage of ~1.23 V at current density of 3 mA/cm² for 10 h. As expected, the battery fabricated with NiO/CoN PINWs shows a considerably stable charging voltage of 2.3 V and a discharging voltage of 1.25 V at current density of 3 mA/cm² with the virtually negligible voltage fading for 300 min [Fig. 4(c)]. Additionally, as shown in Fig. 4(d), the self-made products have a beautiful appearance and good performance. The two-series-connected Zn–air batteries were used to power a blue LED (3.0 V) with excellent operation stability (e.g., without obvious change in brightness more than 48 h) [Fig. 4(d)]. The multiple Zn–air batteries with CoFe₂O₄ nanoparticles as air–cathode can also be used for various applications.

IV. CONCLUSIONS

In summary, we report uniform CoFe₂O₄ nanoparticles with abundant oxygen vacancies and the active crystal face (111) and (110) exposed as efficient bifunctional electrocatalysts for developing high-performance Zn–air batteries. The CoFe₂O₄ nanoparticles exhibit superior performance for HER in acidic media with an onset potential of 20 mV, an overpotential of 45 mV at current density of 10 mA/cm², a rapid kinetic reaction with the lower Tafel slope of 35 mV/dec, and remarkable stability at different current densities not less than 100 h. What is

more, the CoFe₂O₄ nanoparticles also displayed a better performance for HER in basic media with the overpotential of 65 mV (at $j = 10$ mA/cm²). The bifunctional electrocatalytic capacity of CoFe₂O₄ nanoparticles was confirmed by good performance for ORR. Both the onset potential (0.84 V) and half-wave potential (0.67 V) of the CoFe₂O₄ nanoparticles for ORR was closer to that of Pt/C (20%), and more importantly, the ORR catalyzed the CoFe₂O₄ nanoparticles via four electrons processes. Based on the excellent bifunctional electrocatalytic performance, the primary home-made Zn–air batteries were fabricated, showing the OCV of 1.47 V and the maximum power density of 142 mW/cm². Furthermore, the two-series-connected batteries fabricated by CoFe₂O₄ nanoparticles can support a LED to work for more than 48 h. The design of uniform nanoparticles with active crystal face exposed for boosting catalysis should also be providing a promising approach for fabricating multifunctional materials for efficient renewable energy applications.

AUTHOR CONTRIBUTIONS

The article was written through contributions of all authors. All authors have given approval for the final version of the article.

ACKNOWLEDGMENTS

The authors acknowledge the support from the National Natural Science Foundation of China (No. 21571089) and the Fundamental Research Funds for the Central Universities (Izujbky-2016-k02, Izujbky-2016-k09, Izujbky-2016-38).

REFERENCES

1. A.S. Aricò, P. Bruce, B. Scrosati, J-M. Tarascon, and W.V. Schalkwijk: Nanostructured materials for advanced energy conversion and storage devices. *Nat. Mater.* **4**, 366 (2005).
2. S.S. Shinde, C-H. Lee, A. Sami, D-H. Kim, S-U. Lee, and J-H. Lee: Scalable 3-D carbon nitride sponge as an efficient metal-free bifunctional oxygen electrocatalyst for rechargeable Zn–air batteries. *ACS Nano* **11**, 347 (2017).
3. J. Zhang, Z. Zhao, Z. Xia, and L. Dai: A metal-free bifunctional electrocatalyst for oxygen reduction and oxygen evolution reactions. *Nat. Nanotechnol.* **10**, 444 (2015).
4. S. Zhao, H. Yin, L. Du, L. He, K. Zhao, L. Chang, G. Yin, H. Zhao, S. Liu, and Z. Tang: Carbonized nanoscale metal-organic frameworks as high performance electrocatalyst for oxygen reduction reaction. *ACS Nano* **8**, 12660 (2014).
5. Z-Q. Liu, H. Cheng, N. Li, T.Y. Ma, and Y-Z. Su: ZnCo₂O₄ quantum dots anchored on nitrogen-doped carbon nanotubes as reversible oxygen reduction/evolution electrocatalysts. *Adv. Mater.* **28**, 3777 (2016).
6. K. Gong, F. Du, Z. Xia, M. Durstock, and L. Dai: Nitrogen-doped carbon nanotube arrays with high electrocatalytic activity for oxygen reduction. *Science* **323**, 760 (2009).
7. L. Duan, F. Bozoglian, S. Mandal, B. Stewart, T. Privalov, A. Lobet, and L. Sun: A molecular ruthenium catalyst with

- water-oxidation activity comparable to that of photosystem II. *Nat. Chem.* **4**, 418 (2012).
8. C. Cui, L. Gan, M. Heggen, S. Rudi, and P. Strasser: Compositional segregation in shaped Pt alloy nanoparticles and their structural behavior during electrocatalysis. *Nat. Mater.* **12**, 765 (2013).
 9. C. Zhang, S. Hwang, A. Trout, and Z. Peng: Solid-state chemistry-enabled scalable production of octahedral Pt–Ni alloy electrocatalyst for oxygen reduction reaction. *J. Am. Chem. Soc.* **136**, 7805 (2014).
 10. L. Dai, Y. Xue, L. Qu, H. Choi, and J. Baek: Metal-free catalysts for oxygen reduction reaction. *Chem. Rev.* **115**, 4823 (2015).
 11. K. Fominykh, P. Chernev, I. Zaharieva, J. Sicklinger, G. Stefanic, M. Döblinger, A. Müller, A. Pokharel, S. Böcklein, C. Scheu, T. Bein, and D. Fattakhova-Rohlfing: Iron-doped nickel oxide nanocrystals as highly efficient electrocatalysts for alkaline water splitting. *ACS Nano* **9**, 5180 (2015).
 12. Q. Liu, Y. Wang, L. Dai, and J. Yao: Scalable fabrication of nanoporous carbon fiber films as bifunctional catalytic electrodes for flexible Zn-air batteries. *Adv. Mater.* **28**, 3000 (2016).
 13. B. Liu, C. Wu, J. Miao, and P. Yang: All inorganic semiconductor nanowire mesh for direct solar water splitting. *ACS Nano* **8**, 11739 (2014).
 14. J. Mefford, X. Rong, A. Abakumov, W. Hardin, S. Dai, A. Kolpak, K.P. Johnston, and J. Stevenson: Water electrolysis on La_{1-x}Sr_xCoO_{3-δ} perovskite electrocatalysts. *Nat. Commun.* **7**, 11053 (2016).
 15. P. Hiralal, S. Imaizumi, H. Unalan, H. Matsumoto, M. Minagawa, M. Rouvala, A. Tanioka, and G. Amarantunga: Nanomaterial-enhanced all-solid flexible zinc-carbon batteries. *ACS Nano* **4**, 2730 (2009).
 16. F. Cao, M. Zhao, Y. Yu, B. Chen, Y. Huang, J. Yang, X. Cao, Q. Lu, X. Zhang, Z. Zhang, C. Tan, and H. Zhang: Synthesis of two-dimensional CoS_{1.097}/nitrogen-doped carbon nanocomposites using metal-organic framework nanosheets as precursors for supercapacitor application. *J. Am. Chem. Soc.* **138**, 6924 (2016).
 17. Y. Zhu, T. Ma, M. Jaroniec, and S. Qiao: Self-templating synthesis of hollow Co₃O₄ microtube arrays for highly efficient water electrolysis. *Angew. Chem., Int. Ed.* **56**, 1324 (2017).
 18. K. Qu, Y. Zheng, S. Dai, and S. Qiao: Graphene oxide-polydopamine derived N,S-codoped carbon nanosheets as superior bifunctional electrocatalysts for oxygen reduction and evolution. *Nano Energy* **19**, 373 (2016).
 19. T. Ling, D. Yan, Y. Jiao, H. Wang, Y. Zheng, X. Zheng, J. Mao, X. Du, Z. Hu, M. Jaroniec, and S. Qiao: Engineering surface atomic structure of single-crystal cobalt(II) oxide nanorods for superior electrocatalysis. *Nat. Commun.* **7**, 12876 (2016).
 20. T. Ma, J. Cao, M. Jaroniec, and S. Qiao: Interacting carbon nitride and titanium carbide nanosheets for high-performance oxygen evolution. *Angew. Chem., Int. Ed.* **55**, 1138 (2016).
 21. S. Chen, J. Duan, P. Bian, Y. Tang, R. Zheng, and S. Qiao: Three-dimensional smart catalyst electrode for oxygen evolution reaction. *Adv. Energy Mater.* **5**, 1500936 (2015).
 22. J. Duan, S. Chen, M. Jaroniec, and S. Qiao: Heteroatom-doped graphene-based materials for energy-relevant electrocatalytic processes. *ACS Catal.* **5**, 5207 (2015).
 23. H. Shi and G. Zhao: Water oxidation on spinel NiCo₂O₄ nanoneedles anode: Microstructures, specific surface character, and the enhanced electrocatalytic performance. *J. Phys. Chem. C* **118**, 25939 (2014).
 24. X. Gao, H. Zhang, Q. Li, X. Yu, Z. Hong, X. Zhang, C. Liang, and Z. Lin: Hierarchical NiCo₂O₄ hollow microcuboids as bifunctional electrocatalysts for overall water-splitting. *Angew. Chem., Int. Ed.* **55**, 6290 (2016).
 25. C. Xia, Q. Jiang, C. Zhao, M. Hedhili, and H. Alshareef: Selenide-based electrocatalysts and scaffolds for water oxidation applications. *Adv. Mater.* **28**, 77 (2016).
 26. V. Augustyn, P. Simon, and B. Dunn: Pseudocapacitive oxide materials for high-rate electrochemical energy storage. *Energy Environ. Sci.* **7**, 1597 (2014).
 27. R. Wang, J. Lang, Y. Liu, Z. Lin, and X. Yan: Ultra-small, size-controlled Ni(OH)₂ nanoparticles: Elucidating the relationship between particle size and electrochemical performance for advanced energy storage devices. *NPG Asia Mater.* **7**, e183 (2015).
 28. Z. Yu, L. Tetard, L. Zhai, and J. Thomas: Supercapacitor electrode materials: Nanostructures from 0 to 3 dimensions. *Energy Environ. Sci.* **8**, 702 (2015).
 29. Y. Zhao, K. Kamiya, K. Hashimoto, and S. Nakanishi: In situ CO₂-emission assisted synthesis of molybdenum carbonitride nanomaterial as hydrogen evolution electrocatalyst. *J. Am. Chem. Soc.* **137**, 110 (2015).
 30. J. Yin, Q. Fan, Y. Li, F. Cheng, P. Zhou, P. Xi, and S. Sun: Ni–C–N nanosheets as catalyst for hydrogen evolution reaction. *J. Am. Chem. Soc.* **138**, 14546 (2016).
 31. T. Wang, Y. Guo, Z. Zhou, X. Chang, J. Zheng, and X. Li: Ni–Mo nanocatalysts on N-doped graphite nanotubes for highly efficient electrochemical hydrogen evolution in acid. *ACS Nano* **10**, 10397 (2016).
 32. Y. Zhong, X. Xia, F. Shi, J. Zhan, J. Tu, and H. Fan: Transition metal carbides and nitrides in energy storage and conversion. *Adv. Sci.* **3**, 1500286 (2016).
 33. Y. Zhang, B. Ouyang, J. Xu, S. Chen, R. Rawat, and H. Fan: 3D porous hierarchical nickel-molybdenum nitrides synthesized by RF plasma as highly active and stable hydrogen-evolution-reaction electrocatalysts. *Adv. Energy Mater.* **6**, 1600221 (2016).
 34. L. Huang, D. Chen, Y. Ding, S. Feng, Z. Wang, and M. Liu: Nickel–cobalt hydroxide nanosheets coated on NiCo₂O₄ nanowires grown on carbon fiber paper for high-performance pseudocapacitors. *Nano Lett.* **13**, 3135 (2013).
 35. J. Yin, P. Zhou, L. An, L. Huang, C. Shao, J. Wang, H. Liu, and P. Xi: Self-supported nanoporous NiCo₂O₄ nanowires with cobalt-nickel layered oxide nanosheets for overall water splitting. *Nanoscale* **8**, 1390 (2016).
 36. L. An, L. Huang, P. Zhou, J. Yin, H. Liu, and P. Xi: Self-standing high-performance hydrogen evolution electrode with nanostructured NiCo₂O₄/CuS heterostructures. *Adv. Funct. Mater.* **25**, 6814 (2015).
 37. K. Xu, P. Chen, X. Li, Y. Tong, H. Ding, X. Wu, W. Chu, Z. Peng, C. Wu, and Y. Xie: Metallic nickel nitride nanosheets realizing enhanced electrochemical water oxidation. *J. Am. Chem. Soc.* **137**, 4119 (2015).
 38. D. Bediako, B. Lassalle-Kaiser, Y. Surendranath, J. Yano, V. Yachandra, and D. Nocera: Structure-activity correlations in a nickel–borate oxygen evolution catalyst. *J. Am. Chem. Soc.* **134**, 6801 (2012).
 39. J. Kibsgaard, Z. Chen, B. Reinecke, and T. Jaramillo: Engineering the surface structure of MoS₂ to preferentially expose active edge sites for electrocatalysis. *Nat. Mater.* **11**, 963 (2012).
 40. K. Nam, S. Bak, E. Hu, X. Yu, Y. Zhou, X. Wang, L. Wu, Y. Zhu, K. Chung, and X. Yang: Combining in situ synchrotron X-ray diffraction and absorption techniques with transmission electron microscopy to study the origin of thermal instability in over-charged cathode materials for lithium-ion batteries. *Adv. Funct. Mater.* **23**, 1047 (2013).
 41. J. Zhang, L. Qu, G. Shi, J. Liu, J. Chen, and L. Dai: N,P-codoped carbon networks as efficient metal-free bifunctional catalysts for oxygen reduction and hydrogen evolution reactions. *Angew. Chem., Int. Ed.* **55**, 2230 (2016).
 42. H. Jin, J. Wang, D. Su, Z. Wei, Z. Pang, and Y. Wang: In situ cobalt–cobalt oxide/N-doped carbon hybrids as superior

- bifunctional electrocatalysts for hydrogen and oxygen evolution. *J. Am. Chem. Soc.* **137**, 2688 (2015).
43. H. Wang, S. Zhuo, Y. Liang, X. Han, and B. Zhang: General self-template synthesis of transition-metal oxide and chalcogenide mesoporous nanotubes with enhanced electrochemical performances. *Angew. Chem., Int. Ed.* **55**, 9055 (2016).
44. Y. Zhang, B. Ouyang, J. Xu, G. Jia, S. Chen, R. Rawat, and H. Fan: Rapid synthesis of cobalt nitride nanowires: Highly efficient and low-cost catalysts for oxygen evolution. *Angew. Chem., Int. Ed.* **55**, 8670 (2016).
45. Y. Sharma, N. Sharma, G. Rao, and B. Chowdari: Studies on spinel cobaltites, FeCo₂O₄ and MgCo₂O₄ as anodes for Li-ion batteries. *Solid State Ionics* **179**, 587 (2008).
46. T. Ma, S. Dai, M. Jaroniec, and S. Qiao: Metal-organic framework derived hybrid Co₃O₄-carbon porous nanowire arrays as reversible oxygen evolution electrodes. *J. Am. Chem. Soc.* **136**, 13925 (2014).
47. C. McCrory, S. Jung, J. Peters, and T. Jaramillo: Benchmarking heterogeneous electrocatalysts for the oxygen evolution reaction. *J. Am. Chem. Soc.* **135**, 16977 (2013).
48. P. Chen, K. Xu, Z. Fang, Y. Tong, J. Wu, X. Lu, X. Peng, H. Ding, C. Wu, and Y. Xie: Metallic Co₄N porous nanowire arrays activated by surface oxidation as electrocatalysts for the oxygen evolution reaction. *Angew. Chem., Int. Ed.* **54**, 14710 (2015).
49. M. Gao, X. Cao, Q. Gao, Y. Xu, Y. Zheng, J. Jiang, and S. Yu: Nitrogen-doped graphene supported CoSe₂ nanobelt composite catalyst for efficient water oxidation. *ACS Nano* **8**, 3970 (2014).
50. M. Gao, W. Sheng, Z. Zhuang, Q. Fang, S. Gu, J. Jiang, and Y. Yan: Efficient water oxidation using nanostructured α -nickel-hydroxide as an electrocatalyst. *J. Am. Chem. Soc.* **136**, 7077 (2014).
51. M. Gong, Y. Li, H. Wang, Y. Liang, J. Wu, J. Zhou, J. Wang, T. Regier, F. Wei, and H. Dai: An advanced Ni–Fe layered double hydroxide electrocatalyst for water oxidation. *J. Am. Chem. Soc.* **135**, 8452 (2013).
52. J. Bao, X. Zhang, B. Fan, J. Zhang, M. Zhou, W. Yang, X. Hu, H. Wang, B. Pan, and Y. Xie: Ultrathin spinel-structured nanosheets rich in oxygen deficiencies for enhanced electrocatalytic water oxidation. *Angew. Chem., Int. Ed.* **54**, 7399 (2015).
53. F. Lei, Y. Sun, K. Liu, S. Gao, L. Liang, B. Pan, and Y. Xie: Oxygen vacancies confined in ultrathin indium oxide porous sheets for promoted visible-light water splitting. *J. Am. Chem. Soc.* **136**, 6826 (2014).
54. G. Nam, J. Park, M. Choi, P. Oh, S. Park, M. Kim, N. Park, J. Cho, and J. Lee: Carbon-coated core–shell Fe–Cu nanoparticles as highly active and durable electrocatalysts for a Zn–air battery. *ACS Nano* **9**, 6493 (2015).
55. F. Meng, H. Zhong, D. Bao, J. Yan, and X. Zhang: In situ coupling of strung Co₄N and intertwined N–C fibers toward free-standing bifunctional cathode for robust, efficient, and flexible Zn–air batteries. *J. Am. Chem. Soc.* **138**, 10226 (2016).
56. J. Park, M. Park, G. Nam, J. Lee, and J. Cho: All-solid-state cable-type flexible zinc–air battery. *Adv. Mater.* **27**, 1396 (2015).